Plasmon Enhanced Symmetric Mode Generation in Metal-Insulator-Metal Structure with Kerr Nonlinear Effect

Rakibul Hasan Sagor
Islamic University of Technology (IUT)
Board Bazar, Gazipur,
Bangladesh.

ABSTRACT
A time domain simulation algorithm for the investigation of propagation properties of nonlinear Surface-Plasmon-Polaritons (SPP) mode through gallium lanthanum sulphide (GLS) layer in Ag-GLS-Ag waveguide is presented. GLS, a semiconducting chalcogenide glass is known as ultrafast nonlinear device due to their high material non-linearity with strong confinement and dispersion. The time domain simulation algorithm is developed using the Finite Difference Time Domain (FDTD) method. The frequency-dependent dispersion relations as well as third-order non-linearity of GLS glass are modeled using the general polarization algorithm incorporated in the auxiliary differential equation (ADE) technique considering the Kerr nonlinear effect. The dynamics of the whole system is simulated and the effect on SPP propagation is also studied.

General Terms
Finite Difference Time Domain (FDTD), Auxiliary differential equation (ADE), Kerr nonlinear effect.

Keywords
Chalcogenide glass, Surface Plasmon Polaritons (SPP), FDTD method.

1. INTRODUCTION
Surface Plasmon Polaritons (SPPs) have attracted a lot of research in integrated optical circuits and devices due to their ability to overcome the diffraction limit and manipulation of light on a subwavelength scale [1, 2]. A good number of researches have been done to investigate the SPP effect on nonlinear optical devices [3-5]. SPP waveguides with metal-insulator-metal (MIM) configuration have gained an increasing research interest due to their ability to squeeze SPP field into dielectric core below diffraction limit which enables MIM geometry to use it as a plasmonics slot waveguide in nano scale level [6, 7].

Recently SPP behavior in nonlinear optical devices has been suited to investigate the light behavior in nano-scale photonic circuit [8, 9]. However, to stimulate the nonlinear effect, high operational light intensity is necessary [10]. Recently, MIM waveguide with SPP source have been demonstrated experimentally by Koller [11] and Walter [12].

In this paper, the propagation properties of symmetric SPP mode in Ag-GLS-Ag waveguide with Kerr nonlinear effect have been studied and investigated. The dielectric constant of Kerr nonlinear medium (GLS) is changed by varying the pump signal intensity. GLS is one of the Chalcogenide glasses which is ultrafast nonlinear device with high refractive index [13] with a transparency band ranging from 500 nm to 10 μm [14]. The ultrafast high nonlinearity characteristics of GLS glasses combined with silver can be used to propagate SPPs more efficiently, which can be a great contribution in the field of photonics.

The mathematical formulation to represent the nonlinear GLS glass as well as the Silver is done in section 2. A 2-D simulator capable of calculating the propagation dynamics of SPP in nonlinear MIM waveguides is also developed using a FDTD-based time-domain simulation algorithm. In section 3, the discretization of the linear and nonlinear time domain equation is formulated using general ADE-FDTD updating scheme. The specifications and the dimensions of the metal-insulator-meal structure which is considered for this paper is described in section 4. The major outcome and the analytical result of SPP propagation through Ag-GLS-Ag is described in section 5. This paper is concluded in section 6.

2. FORMULATION
Considering material nonlinearity, the frequency-dependent electric flux density can be written as,

$$D(\omega) = \varepsilon_o \varepsilon_\infty E(\omega) + P_{LN(1)}(\omega) + P_{LN(2)}(\omega) + P_{LN(3)}(\omega) \quad (1)$$

$P_{LN(1)}(\omega)$, $P_{LN(2)}(\omega)$ and $P_{LN(3)}(\omega)$ represent first order linear response, second order non-linear response and third order non-linear response respectively. The first order linear response for chalcogenide glass and silver are represented by Lorentz model and multi-pole Lorentz-Drude model which can be written as,

$$P_{LN(1)}(\omega) = \varepsilon_o \left(\frac{\sum_{i=1}^{N} \omega_{qi}}{j\Gamma_i \omega - \omega^2} + \frac{\sum_{k=1}^{M} \omega_{pk}}{\omega_o + j\Gamma_i \omega - \omega^2} \right) E(\omega) \quad (2)$$

where, *N* and *M* represent the number of poles. The second order non-linear response $P_{LN(2)}(\omega)$ is not relevant to this work. The general Lorentzian model is expressed as,

$$P_{LN(1)}(\omega) = \frac{a}{b + jc\omega - d\omega^2} E(\omega) \quad (3)$$

which can be written in the time domain as

$$bP_{LN(1)}(t) + cP'_{LN(1)}(t) + dP''_{LN(1)}(t) = aE(t) \quad (4)$$

The third-order nonlinear polarization can be expressed as the time convolution between the third-order susceptibility function $\chi^{(3)}$ and the electric field. For the simple model consisting of an electron and the core of the atoms, using Born-Oppenheimer approximation [15]

$$P_{NL(3)}(t) = \varepsilon_o \chi_o^{(3)} E(t) \int_{-\infty}^{t} g(t-t') E^2(t') dt' \quad (5)$$

The nonlinear response function $g(t)$ can be expressed as

$$g(t) = \alpha\delta(t) + (1-\alpha) g_r(t) \quad (6)$$

with $g_r(t) = \frac{\tau_1^2 + \tau_2^2}{\tau_1^2 \tau_2^2} \exp\left(-\frac{t}{\tau_2}\right) \sin\left(\frac{t}{\tau_1}\right) u(t)$. The function $u(t)$ is normalized such that $\int_{-\infty}^{\infty} g(t)dt = 1$.

where $\delta(t)$ is the immediate response of electron, $\frac{1}{\tau_1}$ is characteristic frequency of response function of damped oscillation, τ_2 is damping constant and α is the ratio of the Kerr intensity to the total Kerr and Raman nonlinearity. So, including both Kerr and Raman effects the third-order nonlinear polarization can be expressed as,

$$P_{NL(3)}(t) = \varepsilon_o \left\{ \alpha \chi_o^{(3)} E(t)^2 + \left(\chi_R^{(3)} * E(t)^2 \right) \right\} E(t) \quad (7)$$

The instantaneous Kerr effect is represented by the first term on the right hand side of equation (7) and the second term represents the relaxed frequency-dependent Raman scattering with the convolution operation represented by the symbol "*". We define $S(t) = \chi_R^{(3)} * E(t)^2$ such that,

$$S(\omega) = \chi_R^{(3)}(\omega) FT\left\{E(t)^2\right\} \quad (8)$$

where, *FT* represents the fourier transform operation. The general form of $\chi_R^{(3)}(\omega)$ becomes,

$$\chi_R^{(3)}(\omega) = \frac{A\omega_R^2}{\omega_R^2 - 2j\omega\delta_R - \omega^2} \quad (9)$$

where, $A = (1-\alpha)\chi_o^{(3)}(\omega)$, the damping factor $\delta_R = \frac{1}{\tau_2}$, and $\omega_R = \sqrt{\frac{\tau_1^2 + \tau_2^2}{\tau_1^2 \tau_2^2}}$.

The above equations provide time dependent self-consistent solution for the propagation of the input wave through the material where third-order susceptibility, $\chi^{(3)}$ is present. Considering the sensitivity of the signal and material, it is required to solve the equation in their complete form.

3. DISCRETIZATION

3.1 General ADE-FDTD Updating Scheme

The time domain expression of equation (2) can be expressed using general FDTD algorithm [16]**.** From equation (4), the FDTD solution for the first order polarization can be written as

$$P_{LN(1)}^{n+1} = C_1 P_{LN(1)}^{n} + C_2 P_{LN(1)}^{n-1} + C_3 E^n \quad (10)$$

Where,

$C_1 = \frac{4d - 2b\Delta t^2}{2d + c\Delta t}$, $C_2 = \frac{-2d + c\Delta t}{2d + c\Delta t}$ and $C_3 = \frac{2a\Delta t^2}{2d + c\Delta t}$.

The values of C_1, C_2 and C_3 vary by the nature of material (Table I in [16]). The electric field intensity becomes

$$E^{n+1} = \frac{D^{n+1} - \sum_i^N P_{LN(1)}^{n+1}}{\varepsilon_o \varepsilon_\infty} \quad (11)$$

where, D^{n+1} is the update value of electric flux density calculated using the FDTD Yee's algorithm.

3.2 Incorporating $\chi^{(3)}$ in FDTD Algorithm

Using the general alogorithm formulation we can write,

$$S(t)^{n+1} = C_1 S^n + C_2 S^{n-1} + C_3 E^{2n} \quad (12)$$

The update equation representing equation (7) becomes

$$P_{NL(3)}^{n+1} = \alpha_k (E^{n+1})^3 + S^{n+1} E^{n+1} \quad (13)$$

Then the update value of the electric flux density becomes

$$D^{n+1} = \varepsilon_o \varepsilon_\infty E^{n+1} + P_{LN(1)}^{n+1} + \alpha_k (E^{n+1})^3 + S^{n+1} E^{n+1} \quad (14)$$

Equation (14) can be written in the form,

$$a(E^{n+1})^3 + b(E^{n+1})^2 + cE^{n+1} + d = 0 \quad (15)$$

which is a cubic polynomial in E^{n+1} with

$a = 1$, $b = 0$, $c = \frac{(S^{n+1} + \varepsilon_o \varepsilon_\infty)}{\alpha \varepsilon_o \chi^{(3)}}$ and $d = \frac{P_{LN(1)}^{n+1} - D^{n+1}}{\alpha \varepsilon_o \chi^{(3)}}$.

The real solution to equation (15) is given by

$$E^{n+1} = \left(-\frac{d}{2} + \sqrt{\left(\frac{c}{3}\right)^3 + \left(\frac{d}{2}\right)^2} \right)^{\frac{1}{3}} + \left(-\frac{d}{2} - \sqrt{\left(\frac{c}{3}\right)^3 + \left(\frac{d}{2}\right)^2} \right)^{\frac{1}{3}}$$

4. STRUCTURE AND SIMULATIONS

Figure 1 shows the schematic view of the structure under study which is composed of two identical Ag films separated by 100 nm GLS glass. It is required to consider finite GLS film thickness for practical applications. Thinner films show better switching attributes and also are easier to fabricate. For our case, the length of the glass is taken to be 25 μm. The optical properties of silver are modeled using a 6-pole Lorentz-Drude model [17]. The refractive index data for amorphous GLS were derived from ellipsometric measurements which was published in [18]. The dispersion relation of GLS glass was also found in [18].

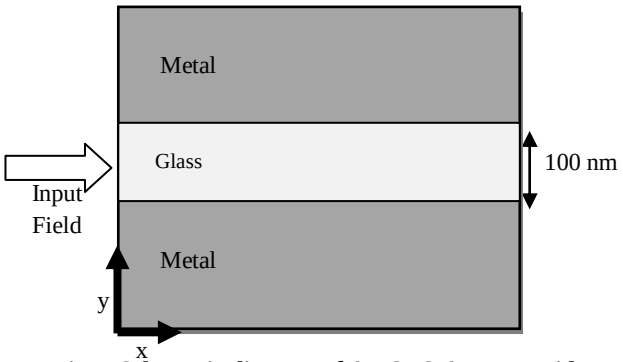

Fig 1: Schematic diagram of Ag-GLS-Ag waveguide used in the simulator.

An excellent agreement with the experimental value is obtained by fitting to a single pole Lorentz model with ε_∞=2.7, ε_s=(2.257)^2, ω_o=0.7x10^{16} rad/s and δ=8.0x10^{11} rad/s. Parameters for nonlinear material are taken as n_2=5.5x10^{-17} m^2/W, $\tau_1 = 12.2fs$, $\tau_2 = 32fs$ and $\alpha = 0.7$. The spatial step

size is taken as $\Delta x = 5nm$, $\Delta y = 5nm$. The time step was set as $\Delta t = \frac{0.95}{c\sqrt{\frac{1}{\Delta x^2} + \frac{1}{\Delta y^2}}}$.

where $c = 3\times10^8 ms^{-1}$.

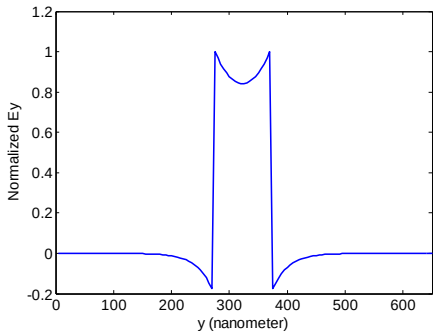

Fig 2: The normalized Ey profile pumped in the device.

To insure the stability with minimum numerical dispersion, the FDTD mesh parameters are set accordingly. A TM polarized wave corresponding to the plasmonics mode shown in figure 2, is pumped at x=0 and time t=0. The plasmonics mode is modulated by a hyperbolic secant pulse having carrier wavelength of 1064 nm and characteristic pulse width of 6 fs (figure 3).

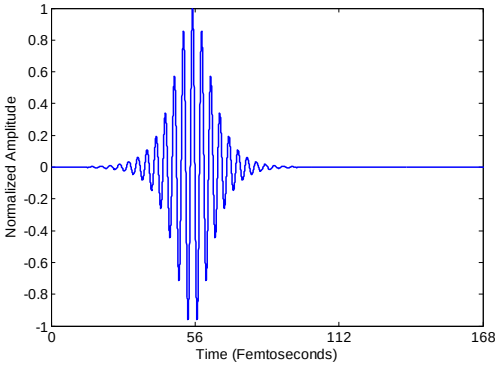

Fig 3: The normalized input pulse in the time domain.

5. RESULTS AND ANALYSIS

Initially the peak amplitude of Ey was set to 2×10^8 V/m. Figure 4 shows evolution of the SPP at different distances in frequency domain. So, it is clear from figure 4 that the nonlinearity has almost no effect on SPP at this input level as the curves almost overlap. In order to stimulate the nonlinear effect, an input with higher peak amplitude must be pumped.

Figure 5 shows the SPP pulse in the frequency domain with non-linear effect for different peak Ey values at the distance of 22.5µm. The frequency domain curves give an insight view of the nonlinear behavior of GLS glass. It is clearly visible that the high input intensity of the signal causes the significant changes in the wavelength of the original signal.

The next set of figures (Figures 6(i)-6(iv)) shows the comparison between the calculated results for input peak Ey amplitude of 2×10^8 V/m and 16×10^8 V/m. Figures 6(i) and 6(iii) are the three dimensional representation of the propagation at different distances.

For high input levels (figures 6(iii) and 6(iv)), the SPP experiences the non-linear effect during the propagation. If we analyze figures 6(iii) and 6(iv), it is observed that initially when the input has a very high intensity, the nonlinearity causes significant changes in the spectral distribution of the input power. As the signal propagates, the strength of each frequency component is modified, making specific frequencies more dominant. For high input intensity, the non-linear effect starts acting on the SPP instantaneously as the Kerr instantaneous effect of non-linearity is considered.

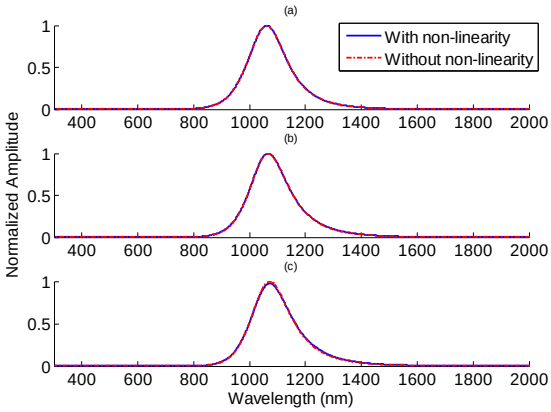

Fig 4: The normalized SPP pulse in the frequency domain without and with non-linear effect for peak Ey value of 2×10^8 V/m at distances of (a) 5µm, (b) 15µm and (c) 22.5µm.

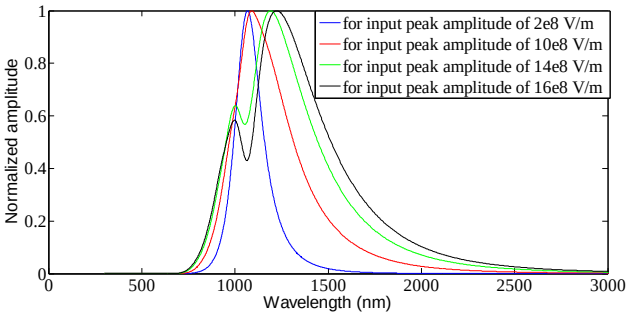

Fig 5: The normalized SPP pulse in the frequency domain with non-linear effect for different peak Ey values at the distance of 22.5µm.

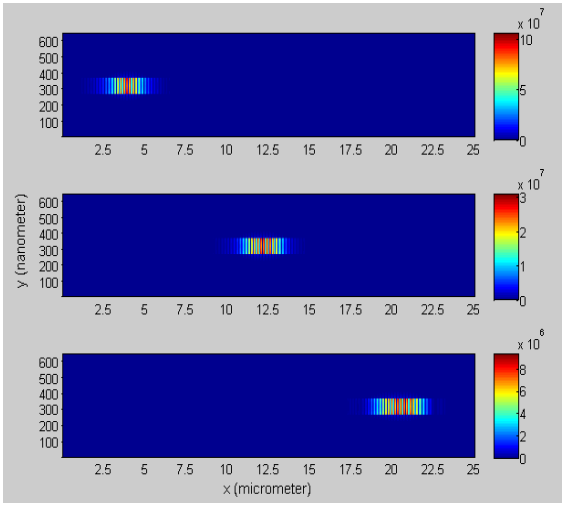

(i)

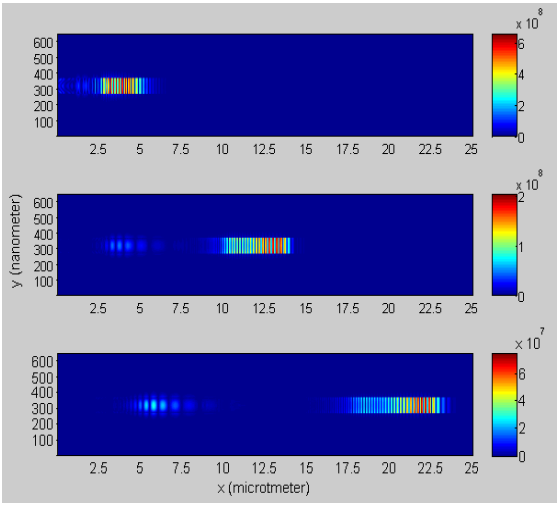

(iii)

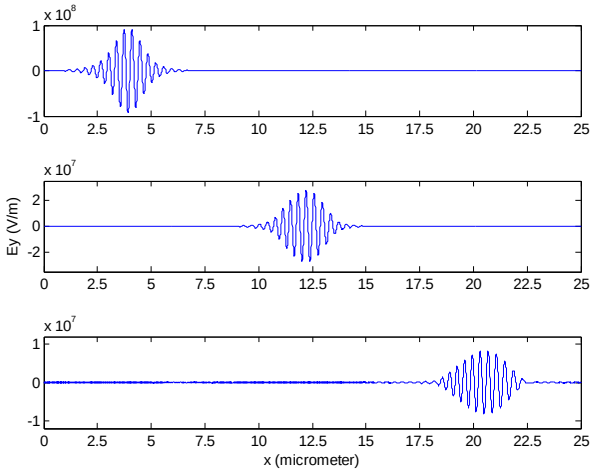

(ii)

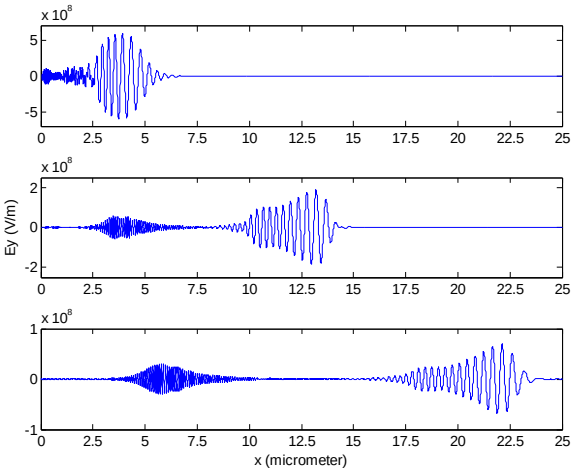

(iv)

Fig 6: Symmetric Ey field distribution at different distances. (i) Three dimensional representation of the propagation at different distances for input peak amplitude of 2×10^8 V/m. (ii) Simulated spatial evolution of optical SPP pulse for input peak amplitude of 2×10^8 V/m at the mid-point of the GLS glass. (iii) Three dimensional representation of the propagation at different distances for input peak amplitude of 16×10^8 V/m. (iv) Simulated spatial evolution of optical SPP pulse for input peak amplitude of 16×10^8 V/m at the mid-point of the GLS glass.

As a result of nonlinear effect, a very interesting feature has been observed. Due to high input intensity, a new propagation mode with different carrier frequency is created. At the beginning of the introduction of the input pulse, due to the excitation of the material nonlinearity a new mode with different frequency starts to develop. Due to the difference in central (carrier) frequency between the two modulated modes, each mode propagates at its own group velocity. The fundamental mode moves at a higher group velocity than the newly created mode. Finally, the fundamental pulse crosses the newly created pulse and the interaction between the two pulses ends. The three dimensional representation of the input fundamental mode and the subsequent generation of slower mode along the structure at different distances are shown in figure 6(iii). Figure 6(iv) shows the simulated spatial evolution of optical SPP pulse along the midpoint of the structure at the same distances. The pulse break-up process is clearly visible for high input intensity of 16×10^8 V/m. This process takes around 15 µm of distance for a 6 fs pulse input.

Figure 7 and 8 show the profile of the slower pulse and faster pulse respectively. The profiles are drawn at the mid-point in the transverse direction. Here, it should be mentioned that, the wavelength of the input pulse was taken to be 1064 nm which is the wavelength of a practical Yag laser. The frequency spectrum for input peak amplitude 16×10^8 V/m, shown in figure 5, gives an insight view of newly created mode and the fundamental mode. It is observed that, the fundamental mode exhibits red shift whereas the slower mode exhibits blue shift from the input frequency. As the signals propagate, due to power loss, the amplitude of the input signal is reduced which causes the waveguide to behave as linear dispersive material. So after a certain distance of propagation, signals are not affected by the nonlinearity of GLS glass.

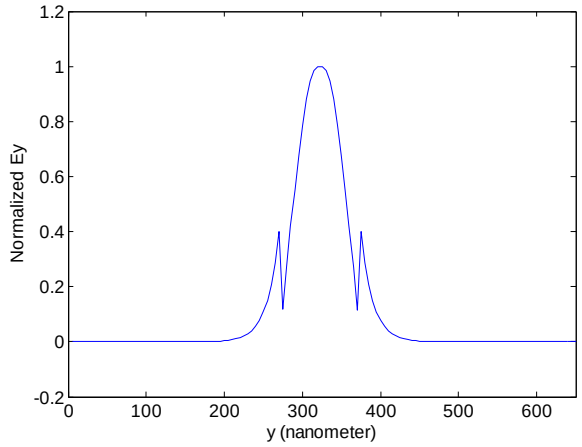

Fig 7: The normalized Ey profile of the slower pulse mode.

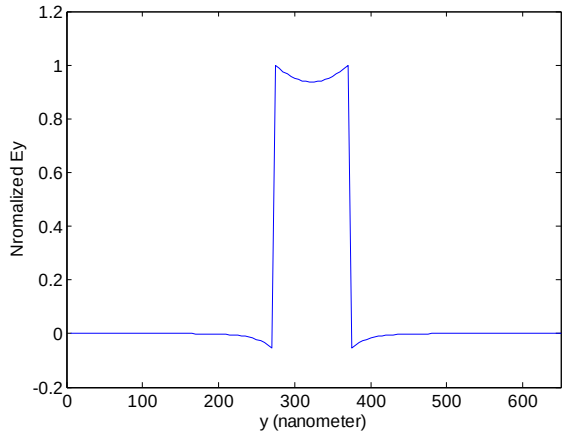

Fig 8: The normalized Ey profile of the faster pulse mode.

6. CONCLUSION

The propagation properties of symmetric SPP mode through Ag-GLS-Ag waveguide are presented considering material dispersion with Kerr nonlinear effect of GLS glass. ADE approach is used to incorporate the frequency-dependent material response into the time domain module. It is clear from the simulation that the non-linearity is stimulated for high input intensity. Results show that the non-linearity of the glass causes the significant changes in spectral distribution of the SPP propagation and demonstrate the pulse break-up phenomenon. With non-linear effect, there is a production of different symmetric mode with different dominant frequencies. This investigation provides further understanding to the coupling between SPP sources and nonlinear plasmonic waveguides. The newly generated dominant frequencies can be used for modulation in optically controlled devices.

7. REFERENCES

[1] W. L. Barnes, *et al.*, "Surface plasmon subwavelength optics," *Nature*, vol. 424, pp. 824-830, 2003.

[2] J. Dionne, *et al.*, "Highly confined photon transport in subwavelength metallic slot waveguides," *Nano letters*, vol. 6, pp. 1928-1932, 2006.

[3] R. Innes and J. Sambles, "Optical non-linearity in liquid crystals using surface plasmon-polaritons," *Journal of Physics: Condensed Matter*, vol. 1, p. 6231, 1989.

[4] W. Dickson, *et al.*, "Electronically controlled surface plasmon dispersion and optical transmission through metallic hole arrays using liquid crystal," *Nano letters*, vol. 8, pp. 281-286, 2008.

[5] T. W. Lee and S. Gray, "Subwavelength light bending by metal slit structures," *Optics Express*, vol. 13, pp. 9652-9659, 2005.

[6] J. Dionne, *et al.*, "Plasmon slot waveguides: Towards chip-scale propagation with subwavelength-scale localization," *Physical Review B*, vol. 73, p. 035407, 2006.

[7] Y. Gong, *et al.*, "Broad-bandgap and low-sidelobe surface plasmon polariton reflector with Bragg-grating-based MIM waveguide," *Optics Express*, vol. 17, pp. 13727-13736, 2009.

[8] Z. J. Zhong, *et al.*, "Sharp and asymmetric transmission response in metal-dielectric-metal plasmonic waveguides containing Kerr nonlinear media," *Optics Express*, vol. 18, pp. 79-86, 2010.

[9] C. Min, *et al.*, "All-optical switching in subwavelength metallic grating structure containing nonlinear optical materials," *Optics letters*, vol. 33, pp. 869-871, 2008.

[10] G. A. Wurtz and A. V. Zayats, "Nonlinear surface plasmon polaritonic crystals," *Laser & photonics reviews*, vol. 2, pp. 125-135, 2008.

[11] D. Koller, *et al.*, "Organic plasmon-emitting diode," *Nature Photonics*, vol. 2, pp. 684-687, 2008.

[12] R. J. Walters, *et al.*, "A silicon-based electrical source of surface plasmon polaritons," *Nature Materials*, vol. 9, pp. 21-25, 2009.

[13] B. J. Eggleton, "Chalcogenide photonics: fabrication, devices and applications Introduction," *Optics Express*, vol. 18, pp. 26632-26634, 2010.

[14] Y. West, *et al.*, "Gallium lanthanum sulphide fibers for infrared transmission," *Fiber & Integrated Optics*, vol. 19, pp. 229-250, 2000.

[15] R. Hellwarth, "Third-order optical susceptibilities of liquids and solids," *Progress in Quantum Electronics*, vol. 5, pp. 1-68, 1979.

[16] M. A. Alsunaidi and A. A. Al-Jabr, "A general ADE-FDTD algorithm for the simulation of dispersive structures," *Photonics Technology Letters, IEEE*, vol. 21, pp. 817-819, 2009.

[17] A. D. Rakic, *et al.*, "Optical properties of metallic films for vertical-cavity optoelectronic devices," *Applied Optics*, vol. 37, pp. 5271-5283, 1998.

[18] Z. L. Sámson, *et al.*, "Chalcogenide glasses in active plasmonics," *physica status solidi (RRL)-Rapid Research Letters*, vol. 4, pp. 274-276, 2010.